Materials Advances

ROYAL SOCIETY OF CHEMISTRY

PAPER

Published on 06 July 2026

Cite this: DOI: 10.1039/d6ma00854b

Electrostamping method for plating copper, nickel, tin, zinc and brass

Afua Atta-Poku,[a] Juli Hancock,[a] Andrew Durst,[a] Anderson Hofstedt,[a] Jason P. Shaw[b] and Troy K. Townsend *[a]

Received 11th June 2026,
Accepted 20th June 2026

DOI: 10.1039/d6ma00854b

rsc.li/materials-advances

Metal electroplating is utilized widely across multiple industries and has been adapted to meet diverse industrial applications by using aqueous or non-aqueous liquid electrolytes containing a submerged workpiece under continuous stirring in a bath or flow-through reactor. However, submersion restricts plating sensitive materials; and large objects require a larger volume liquid bath to scale with the size of the object. In response to this, a novel electrostamping plating technique is explored using viscous dehydrated metal salt paste electrolytes painted on top of the workpiece. Here, the cathode surface can be plated without submerging in a liquid bath, providing a proof of concept option for surface plating of large, irregular, or water sensitive objects. Building on previous work with nickel-composites, this research was expanded to include other metals common to the plating industry including α-Ni, α-Cu, α-Zn, and β-Sn, along with Cu|Zn brass alloys. Following electrostamping coatings under 5, 10 and 20 mA cm^{-2} for 10 or 20 min, plated film masses were recorded to calculate cathode current efficiencies, and microscale and nanoscale surface morphology were visualized with optical and atomic force microscopy. Crystallinity and phase were identified with XRD, and XRF was used to measure elemental ratios of the brass alloys. The method was found to produce smooth crystalline metal deposits (RMS ~250 nm) with high current efficiencies (>90%), providing evidence to suggest a new method that should be investigated for specialized applications in modern engineering and manufacturing.

Introduction

Metal electroplating is critical to technological advances and everyday production in electronics, automotive and aerospace sectors with a global market size of 21.47 billion USD and an expected rise to 33.44 billion by 2034.[1,2] Current aqueous and non-aqueous electroplating is limited to submerging a conductive object in a liquid bath, which places constraints on the size and resistance of the item to aqueous or organic fluids.[3–6] While non-aqueous solvents for example: ionic liquids, deep-eutectic solvents and super critical carbon dioxide offer a wider electrochemical window for reactive metals, these solvents often require heating and attention to air-exposure to avoid electrolyte oxidation. In addition, typical aqueous electroplating requires wastewater treatment for heavy metals, aqueous counterions and toxic metal–organic complexes which is priced between 0.35 and 4.45 USD per m^3 of liquid waste.[7–10] While large items are routinely electroplated industrially, they require a corresponding volume scale-up for the liquid electrolyte. Given the global demand for electroplating and diminishing clean fresh water,[7] investigating new methods to target a reduction in wastewater is needed.

Metal deposition alternatives to liquid electroplating include vapor deposition methods (*i.e.* physical and chemical vapor deposition); however, these methods require pure metal sources and vacuum pressures, which is generally not cost-effective for large scale production.[11] Other commercially used liquid-based spot-deposition methods include brush plating and jet plating, which involve flowing liquid electrolyte (34–68 litres per minute) where the work-piece is often spinning while in contact with a wand containing an absorbent cloth and applied current.[12,13] However, these processes also produce aqueous waste after the electrolyte is reused until it is spent. Considering bottom-up fabrication advances in a multitude of additive manufacturing methods of plastics and metals[14] and the solution printing of electronics,[15] traditional electroplating methods require adaptability for rapid spot plating of the work piece without submersion in a bath. Likewise, when considering top-down post-processing of oversized items, for example repairing the panel of an aircraft[16,17] or applying anti-corrosion coatings for sustainable bridge maintenance, versatile and effective spot plating methods are needed to avoid the electrolyte bath requirement.[18,19]

[a] Department of Chemistry and Materials Science St. Mary's College of Maryland Goodpaster Hall, 47645 College Dr, St. Mary's City, MD 20686, USA. E-mail: tktownsend@smcm.edu
[b] Paradigm Max Q, 50 Tech Parkway, Ste 201, Stafford, VA 22556, USA

In our previous reports, a nickel composite electrostamping process was demonstrated, where phosphor powders were included in the deposit.[20,21] This method was inspired by the dehydrated electrolyte paste common to Leclanché battery cells, where surface plating can be obtained from a stagnant electrolyte paste. The viscous electrolyte was previously found to deposit a metal finish while also trapping large (87 ± 30 μm) uncharged composite particles at high loading amounts, which are traditionally difficult to incorporate.[22–29]

Following from this demonstration with nickel composites, the next logical step forward would be to investigate electrostamping of pure metals; however, currently the authors are not aware of previous demonstrations of electroplating pure or mixed metals from viscous dehydrated electrolyte pastes without composites. In addition, while this method could be used industrially to reduce wastewater, it is also equally interesting for its ability to spot coat metals onto surfaces regardless of their size, which would be appealing for additive manufacturing of electronic/structural hybrid printing and also for post-processing of the surfaces of large assembled structure or vehicles. Because the process does not involve submersion in a liquid (aqueous or non-aqueous), it is also compatible with mid-assembly production of electronic devices.

In this report, we investigate electrostamping of pure nickel, copper, zinc and tin. In addition, molar ratios of copper and zinc were mixed together in an attempt to form a brass alloy. Dehydrated divalent metal salts were formulated into a viscous paste and applied to a clean and acid-activated substrate. An anode was cleaned and placed on top of the paste before the metal was deposited under constant current. Resulting coatings were cleaned with water, and their surface morphology was visualized with optical and atomic force microscopy. Their crystallinity and phase were characterized by X-ray diffraction, and X-ray fluorescence spectroscopy was used to verify the elemental composition of the Cu|Zn coatings (Scheme 1A). A general comparison of this technique with traditional bath plating is also provided (Scheme 1B), highlighting key distinctions.

Results and discussion

Pure metal deposits

Following electrostamping onto nickel plates and rinsing with water, the resulting metal films appeared generally smooth and uniform over the 9 cm^2 surface area (photos in Fig. 1). Slight discolorations are attributed to the formation of thin layers of passive native oxides following removal of the plating from the paste and exposure to air. The optical microscope (Fig. 1) and atomic force microscope (Fig. S3–S6) images confirmed the smooth surface where nickel and copper appeared to be less rough than zinc and tin, and area roughness ranged across all samples from 246 ± 68 nm for nickel and 865 ± 312 nm for tin. These roughness values were found to be rougher than the as-received (31 nm) and the acid-prepped nickel substrates (192 nm, Fig. S9). Generally, roughness also increased with applied current potentially due to kinetically favoured rapid deposition leading to microscale surface features.

X-ray diffraction patterns revealed crystalline metals for each case, and samples were indexed to the expected planar reflections for face centered cubic (FCC) crystals (α-Ni, α-Cu, α-Zn) or hexagonal close packed for β-Sn (Fig. 2).[30] All samples contain the nickel reflections of the common substrate, and all samples appeared to be free of contaminates, alternative crystal phases or oxides. This is expected because each metal phase observed in the XRD pattern is most stable under ambient conditions.[31]

The masses of the coatings were recorded and compared across the various experimental conditions of time (10 or 20 min) and applied current (5, 10 and 20 mA cm^{-2}) revealing

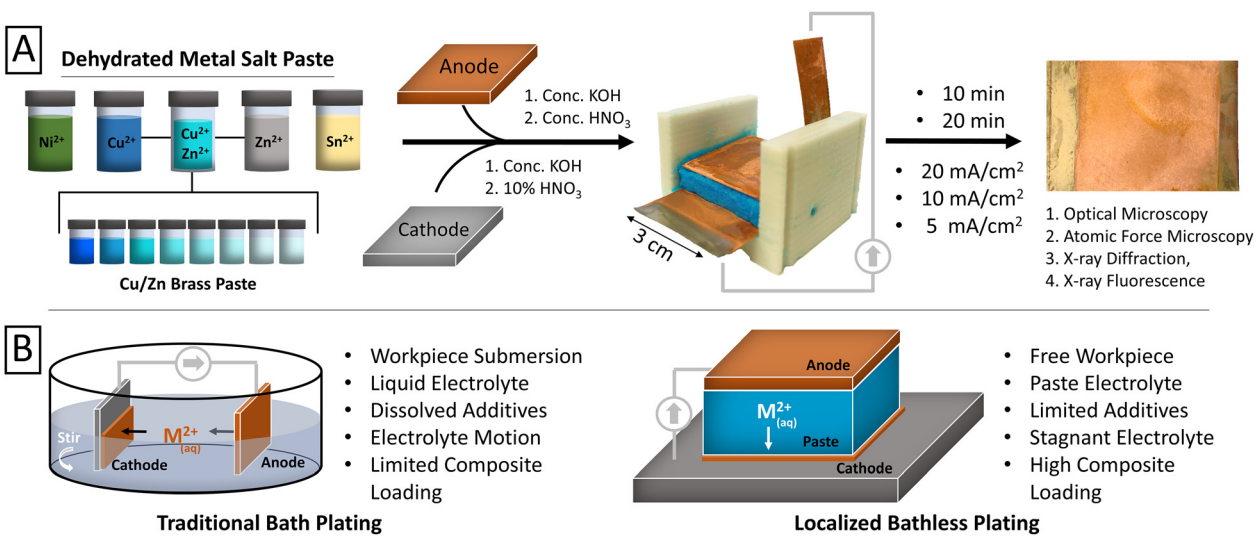

Scheme 1 Dehydrated metal salt pastes containing divalent metals of nickel, copper, zinc, tin or alloy molar ratios of copper and zinc were added to clean and activated cathode substrates with anode top contact to be electroplated without a bath for 10 or 20 min at 20, 10 or 5 mA cm^{-2} followed by materials characterization [A] and a comparison between traditional bath plating and electrostamping plating [B].

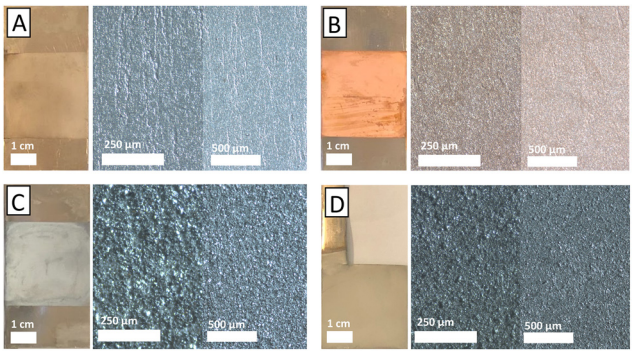

Fig. 1 Plated metal coupon photos and optical microscope images with split magnification panels plated onto nickel substrates for 10 min under a constant current of 20 mA cm^{-2} and exposed to dehydrated salts of Ni^{2+} [A], Cu^{2+} [B], Zn^{2+} [C] and Sn^{2+} [D]. Additional photos, optical and atomic force microscope images for all six treatments of 10 min *vs.* 20 min at 20, 10 and 5 mA cm^{-2} are provided in Fig. S1–S6.

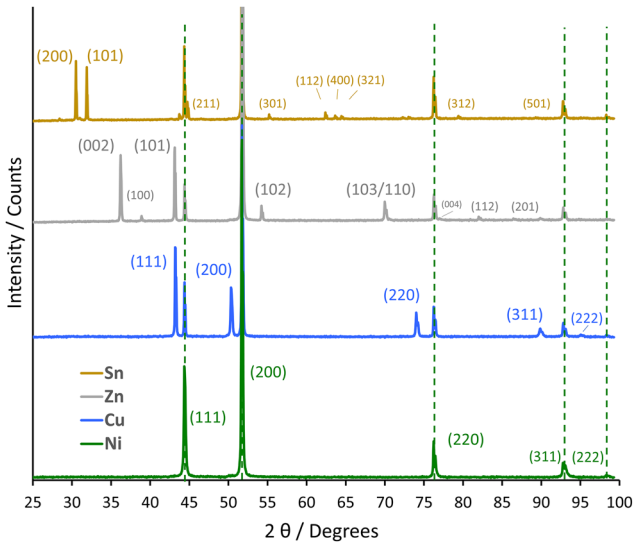

Fig. 2 X-ray diffraction patterns of metals plated onto a nickel substrate including indexed reflections for electrostamping for 10 min under a constant current of 20 mA cm^{-2} in the presence of Ni^{2+}, Cu^{2+}, Zn^{2+} and Sn^{2+} salt paste resulting in the formation of α-nickel (green), α-copper (blue), α-zinc (grey) and β-tin (gold), respectively.

the expected trend where mass of the plating scales directly with the applied current (Fig. 3). Like the mass, thicknesses scaled well ($R^2 > 0.95$) with applied current with final deposits ranging from 1–2 μm under 5 mA cm^{-2} and up to 8–9 μm under 20 mA cm^{-2}, after 20 min (Fig. S7). Deposit mass was plotted along with the theoretical plating mass yield (where $\phi = 1$) calculated from Faraday's law of electrolysis[32] using eqn (1)

$$w = \frac{\Phi I t M}{F z} \quad (1)$$

where w is the mass of metal deposited (g), ϕ is the cathode current efficiency, I is the applied current (A), t is the coating time (s), M is the molar mass (g mol^{-1}), F is Faraday's constant

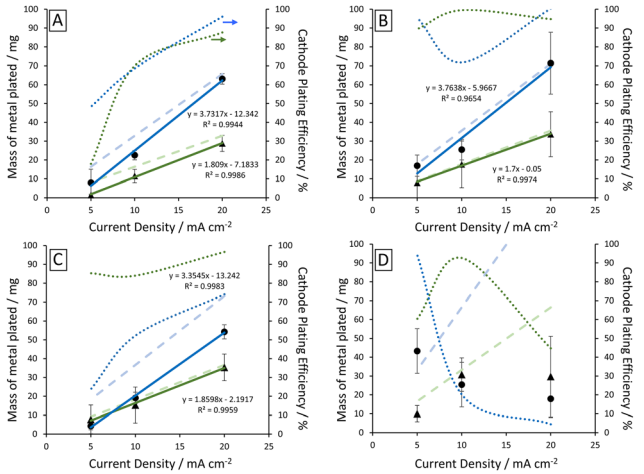

Fig. 3 Mass of metal deposited under constant current densities of 5, 10 and 20 mA cm^{-2} for 10 min (green, triangles) and 20 min (blue, circles) including their calculated theoretical mass yield (dashed blue for 20 min or green for 10 min) and the cathode current efficiency averages (dotted green for 10 min and dotted blue for 20 min coatings) with error bars representing standard error of the mean (n = 3) for 10 min (green dotted) and 20 min (blue dotted) for plating from dehydrated salts of Ni^{2+} [A], Cu^{2+} [B], Zn^{2+} [C] and Sn^{2+} [D].

(96 485 coulombs per mole) and z is the charge of the metal ion. Likewise, the average thickness t of the deposit can be calculated from eqn (2) by dividing the mass by the density ρ and area A of the metal deposited.

$$t = \frac{w}{\rho A} \quad (2)$$

For all metals except Sn, the experimental mass yield increased with current density. Both nickel and copper tracked well with the theoretical expected amounts. Zinc plated for 20 min fell under the expected masses, which may be due to its unfavourable standard reduction potential compared to the other metals. The Sn coatings were crystalline as determined from the XRD patterns, but their deposition did not scale with duration or applied current. This could be attributed to the harsh acidic conditions of the sulfuric acid used for this material,[33] whereas the other metals were deposited from pastes with more moderate pH values [(Ni 2–4.5),[34] (Cu 4–5),[35] (Zn 5–6)[36]] using boric acid (pK_a = 9.2) to buffer the acidic metal cations. While the other metals were able to build upon previous layers at these pH ranges, the Sn-coatings exposed to concentrated sulfuric acid would be expected to simultaneously dissolve during deposition, which is supported by the observed stochastic and unpredictable deposits (Fig. 3D). Electrostamping in its current form was found to be unsuitable for Sn deposition; however, this may be addressed through optimization adapted from traditional aqueous bath plating. For example, electrolyte additives may be needed to improve the electrostamping Sn deposition under acidic conditions including organic compounds to improve the surface morphology, surfactants to promote polarizing effects on the electrode and Sn^{2+} oxidation inhibitors.[37]

The cathode current efficiency (φ) is an indication of the quality of the conversion from electrical power to metal deposition and was calculated using eqn (3)

$$\text{Current efficiency (\%)} = \frac{\text{experimental deposit mass}}{\text{theoretical deposit mass}} \times 100 \quad (3)$$

where the theoretical deposit mass (w) was found from eqn (1).

The plating efficiency increases with the applied current for most samples, and ranged between 20% for low currents and up to >90% for higher currents (Fig. 3A–C). Considering this range, the industrial practicality of this process should be conducted with applied currents around 20 mA cm^{-2} as these plating efficiencies were generally in agreement and just under their bath-plating equivalents found in the literature (90–97%).[34–36,38] In contrast, plating efficiencies scale lower with applied current density below 20 mA cm^{-2}, which may be due to a kinetic competition formed between the slow rate of metal deposition *vs.* hydrogen evolution as a consequence of the Butler–Volmer relationship.[39] For this reason, for example, nickel plating is typically deposited in the range of 10–60 mA cm^{-2}.[3]

Overall, copper plating efficiencies remained high, which is an expected consequence of its thermodynamically favourable reduction potential. However, variations in plating mass were larger relative to Ni and Zn (Fig. 3B error bars) and a drop in current efficiency was observed at 10 mA cm^{-2} during the 20 min plating. These variations are attributed to the formation of a passivating layer on the copper anode (owed to its colourful surface) following plating (Fig. S10). An XRD pattern of the anode revealed the presence of hydrated copper sulfate, cuprous and cupric oxide (Fig. S10C). This excessive oxidation is expected as the anode is exposed to air during this process, instead of being protected from excessive oxidation while submerged in an aqueous bath. Longer exposure times and higher currents led to runaway oxidation of the copper anode, eventually halting the plating process beyond 20–30 min (Fig. 3B and 4B). Given the expected variability of plating stability as discussed previously, the plating efficiency for tin was quite low (<20%) as a result of the lower-than-expected mass yield across all currents and times (Fig. 3D).

The voltage change over time during the plating was monitored with chronopotentiometry where higher applied currents resulted in higher voltages according to Ohm's law (Fig. 4). The voltage remained constant over the ~30 min period for each metal and each applied current, with the exception of copper which was stable for the lower currents but unstable at 20 mA cm^{-2} (Fig. 4B). This result reflects the general variation observed in plating mass for copper (Fig. 3B error bars) and is attributed to the formation of passivating oxide on the anode while exposed to air on the top of the platting structure. Periodic rises in voltage were also observed for copper. Considering the formation of passivating oxide films, which have Pilling-Bedworth ratios in the protective range (~1.65), this scale may become unstable under condition of resistive heating and exposure to the aqueous sulfate electrolyte. This environment may lead to periodic formation and dissolution of the oxide scale and requires further investigation.

The average required voltages were found to increase with applied current for each metal with good correlation following

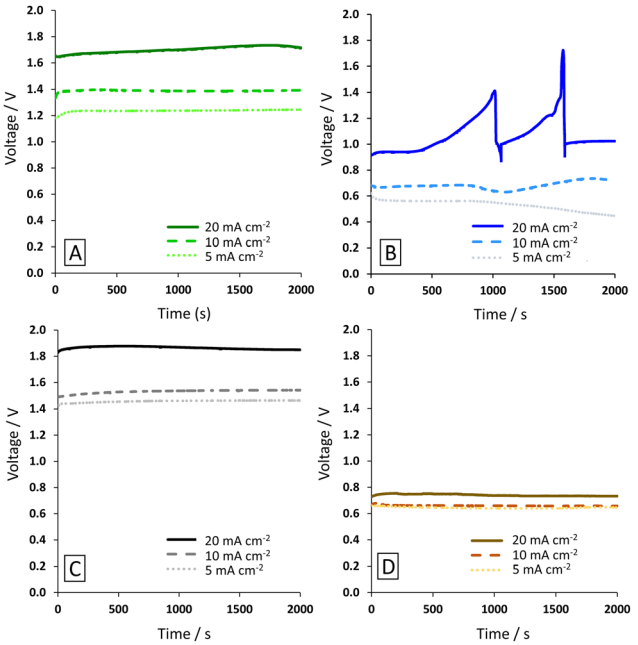

Fig. 4 Chronopotentiometry scans over time under constant current densities of 5 mA cm^{-2} (dotted), 10 mA cm^{-2} (dashed) and 20 mA cm^{-2} (solid line) to monitor voltage changes during plating from dehydrated salts of Ni^{2+} [A], Cu^{2+} [B], Zn^{2+} [C] and Sn^{2+} [D].

Ohm's Law (Fig. 5A). The ordering of the metals from highest voltage to lowest is explained by their standard reduction potentials, which also scaled well with the voltages observed during plating (Fig. 5B). As the standard reduction potential of each metal changes to favour spontaneous reduction, the voltage required to plate them decreases under constant current conditions. This trend is also generally in agreement with the ordering of current efficiencies observed in Fig. 3A–C.

This matches well with theory because it is expected that copper having the highest reduction potential (+0.34 V *vs.* SHE, $\Delta G = -65.6$ kJ mol^{-1}) would be reduced with the lowest amount of resistance given that its reduction onto nickel substrates is naturally spontaneous under ambient conditions. Conversely, the other metals are not spontaneously reduced and require an external applied current, for example zinc is the least spontaneous

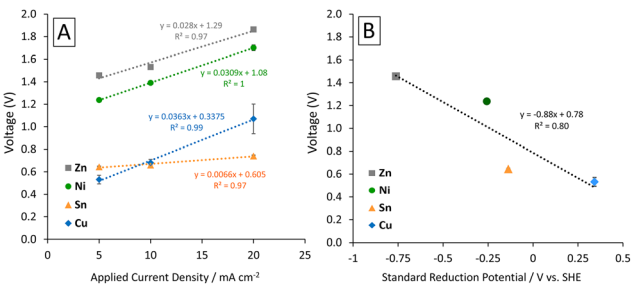

Fig. 5 Average voltages with error bars indicating standard error of the mean recorded from the electrostamping chronopotentiometry plating process plotted as a function of applied current [A] and average voltage under 5 mA cm^{-2} applied current for each metal in relation to their standard reduction potentials [B].

to reduction ($E = -0.76$ V *vs.* SHE, $\Delta G = +146.6$ kJ mol^{-1}) and has the highest voltage requirement to deposit.

Mixed metal deposits: brass alloys

Following positive results of individually plating pure metals of copper and zinc, combinations of Cu^{2+} and Zn^{2+} salts were tested for their potential for plating alloys of Cu|Zn brass metal. Brass alloys with low zinc content below 40% are α phase under ambient conditions and contain β phase between 40–60% Zn content.[40,41] While others have demonstrated aqueous bath plating of brass using a variety of counterions including cyanide[42] and non-cyanide[43,44] alternatives, attempts in our lab to adapt these to electrostamping led to various levels of success. In order to maintain consistency and decrease variability, the platings reported here were formed from dehydrated metal ion pastes that were not changed from their original pure metal recipes of copper sulfate, zinc chloride and boric acid.

Interestingly, as a result of the large difference in reduction potential between copper and zinc (*Δ* 1.10 V), the driving force for spontaneous deposition of copper ions out-competes zinc by a factor of 212 kJ mol^{-1} and $\Delta K_{eq} \sim 10^{26}$. Based on this theory, an attempt was made to leverage statistical favour for zinc incorporation into the copper matrix using Le Chatelier's principle. Ratios in the coating paste varied on the low end from 30% Zn to 90, 95 and 99% Zn on the upper end. The higher loading amounts in the precursor paste was hypothesized to produce the target loading of zinc in the deposit for α-brass given the propensity of copper to spontaneously deposit in place of zinc.

Following deposition and rinsing the samples with water, optical microscope images were taken revealing a color gradient from copper (Fig. 6A,a) to zinc (Fig. 6H,h) and generally smooth and uniform deposits (Fig. 6). Atomic force microscope images measured surface area roughness values smoother for higher zinc content ranging from 142 ± 39 nm for 99Zn:1Cu up to 708 ± 199 nm for 30Zn:70Cu (Fig. S8).

Following from pure copper (100Cu|0Zn) and viewing the trend incrementally to 99% zinc loaded pastes, the copper reflections in the XRD patterns (Fig. 7) decrease with zinc loading and crystalline zinc is not present, with the exception of 30 and 50% zinc where a small peak was observed at 36.67° 2θ for Zn (002). This indicates that zinc metal was plated separately for these samples and may form regions of zinc plating where zinc was not incorporated uniformly throughout the deposit. However, there were no zinc peaks observed for the other reflections expected for zinc metal, providing evidence instead to support the formation of crystalline ZnO with wurtzite hexagonal structure (101 reflection, ~36.26° 2θ).[45] This could be possible given that the plating electrodes experience resistive heating and ZnO formation has been observed at temperatures as low as 25C.[46] As the loading of Cu^{2+} in the $Cu^{2+}|Zn^{2+}$ paste decreases, it is reasonable to observe a corresponding reduction in peak intensity of the Cu metal reflections of the resulting plating.[47] Indeed, as expected, there is a negative linear correlation ($R^2 = 0.88$) between Cu (111) peak area and the Zn loading in the precursor paste. However, another possibility is that the presence of excess Zn^{2+} is promoting the deposition of amorphous copper instead of brass.

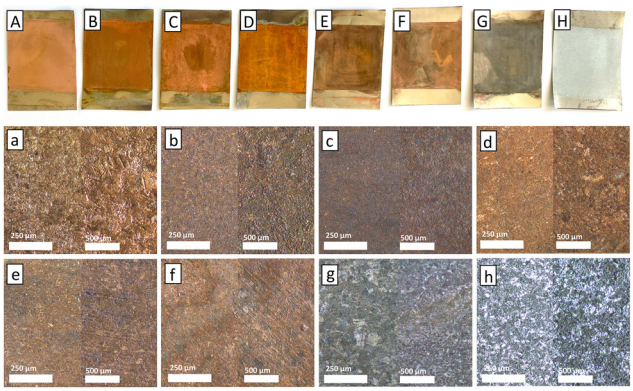

Fig. 6 Plated metal coupon photos [A–H] and corresponding optical microscope images with split magnification panels [a–h] plated onto nickel substrates for 10 min under a constant current of 10 mA cm^{-2} and exposed to dehydrated salts of Cu^{2+} and Zn^{2+} mixed together in molar ratios of Cu|Zn of 100|0 [A,a], 70|30 [B,b], 50|50 [C,c], 30|70 [D,d], 10|90 [E,e], 5|95 [F,f], 1|99 [G,g] and 0|100 [H,h]. Atomic force microscope images are provided in Fig. S8.

The formation of crystalline brass can be determined by XRD where the lattice parameter (as derived from the 2θ reflection angle) should scale with Zn loading in the alloy.[48,49] However, brass undergoes an α/β transition around

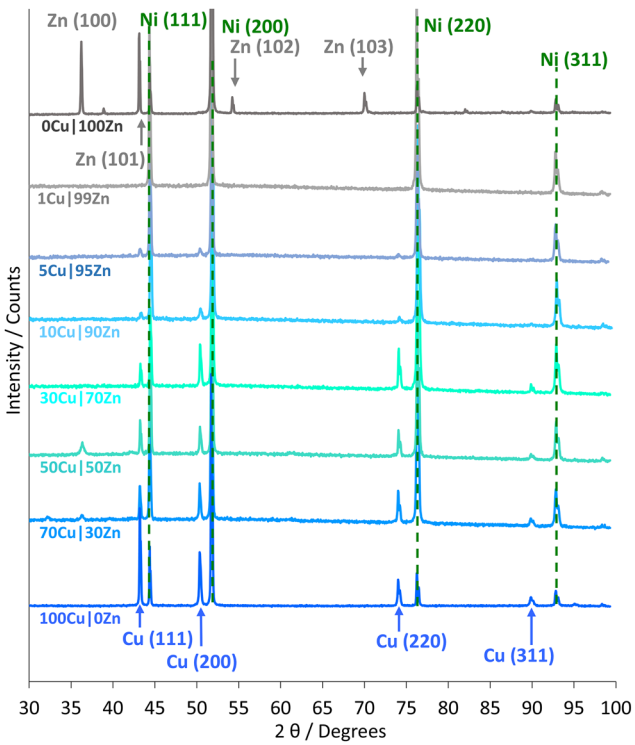

Fig. 7 X-ray diffraction patterns of metals plated onto a nickel substrate including indexed reflections for the electrostamping deposition for 10 min under a constant current of 10 mA cm^{-2} in the presence of Cu^{2+} and Zn^{2+} salt paste mixtures with Cu|Zn molar ratios of 100|0, 70|30, 50|50, 30|70, 10|90, 5|95, 1|99 and 0|100.

37% Zn loading, confounding the determination of loading from the peak angle, because the change in crystal structure (FCC → BCC) does not allow for a linear tracing of lattice change by Vegard's Law of mixtures.[50] Theoretical Cu peak locations are also very near brass reflections, for example there is a difference of only 0.2° 2θ for 90Cu|10Zn *vs.* pure Cu, with brass reflections having a slightly smaller angle due to the larger atomic radius of Zn. While the presence of crystalline material and the loss of crystalline Cu as Zn loading increases was verified by XRD, this spectroscopy alone was unable to verify the formation of brass or quantify the Zn loading in the plating.

To determine the relative Zn to Cu content in the electrostamped coatings, X-ray fluorescence (XRF) spectra were taken of the brass samples, and the Zn content was plotted with the theoretical expected loading from the paste (Fig. 8). Based on the results of the elemental analysis, the large Zn content in the paste did successfully translate to higher loadings in the deposit, although interestingly this did not scale linearly. For example, Zn^{2+} loadings as high as 95% did not allow for plating of Zn metal above 10%. However, with Zn^{2+} loadings at 96% Zn and higher, the resulting deposit jumped to 42% Zn.

This suggests that there is a narrow range of Zn content in the slurry between 95–96% where Zn plating becomes statistically competitive with copper whereas on the lower end of this range at 95% Zn electrolyte content, elemental analysis revealed a deposition of 3.7%. Increasing this by merely 1 percent to 96% Zn, led to a substantial increase in Zn content in the coating. This narrow range may indicate the threshold that separates the preferential plating of copper *vs.* zinc. More research is needed to target mid-range Zn loadings in the platings and may benefit from the investigation of using additives that have been proven for successful brass plating in a liquid bath.[42,43]

Combining the XRF Zn ratios with the XRD results, it is reasonable to suspect that because the Cu XRD peak intensities decrease with Zn loading, formation of crystalline Cu phases are interrupted by the addition of excess Zn, creating the presence of amorphous Cu or brass at higher Zn loadings. Based on this, the electrostamping method provided a proof-of-concept option for alloy deposition; however, more research is required to refine and optimize this new process to verify the crystallinity and tune the atomic ratio of the binary phase.

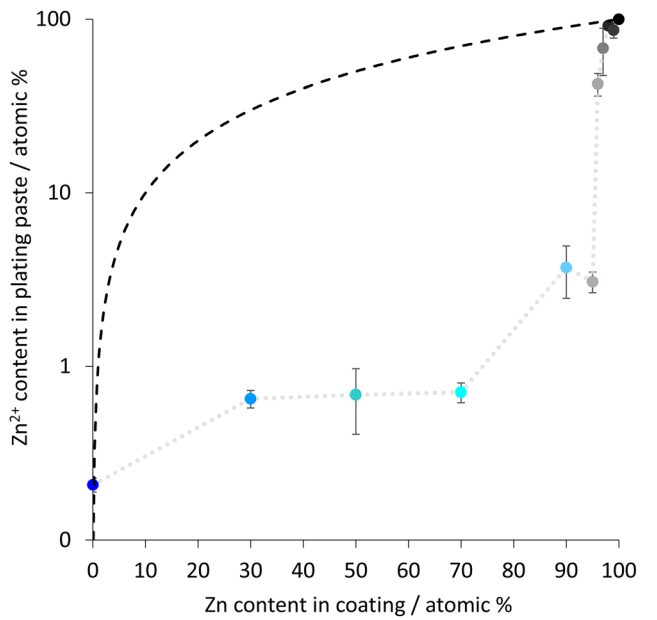

Fig. 8 X-ray fluorescence point-scan data of metal coupons plated with mixtures of Cu^{2+} and Zn^{2+} showing elemental composition of the resulting deposit *vs.* the molar composition of the precursor paste. Error bars denote standard error of the mean (n = 3). Theoretical expected deposit compositions Zn/(Zn + Cu) by mole are provided as a reference (black, dashed).

Large area deposit: application of electrostamping nickel coating on steel

In order to demonstrate the potential applicability of thismethod on coating large surfaces, for items that are too large or otherwise incompatible with submerging in a bath, a large area (144 cm^2) electrostamping deposition was conducted (Fig. 9) on the benchtop in air, at room temperature and without submerging the work piece. It should be noted that this dimensions of this object (and objects much larger) could alternatively be plated in a bath, but this steel sheet was used as a representation for a surface coating that could be deposited on a prohibitely large object, for example a built structure like a bridge or an assembled item in the example of a aircraft panel. A steel plate was cleaned, and a square surface was taped off before adding dehydrated Ni^{2+} paste and a Ni anode large enough to cover the surface (Fig. 9B). Following deposition and to further demonstrate a potential application for this coating method on the corrosion resistance of steel, the nickel-plated coupon was placed outside and exposed to environmental weather conditions for 70 days. This treatment led to the corrosion of the

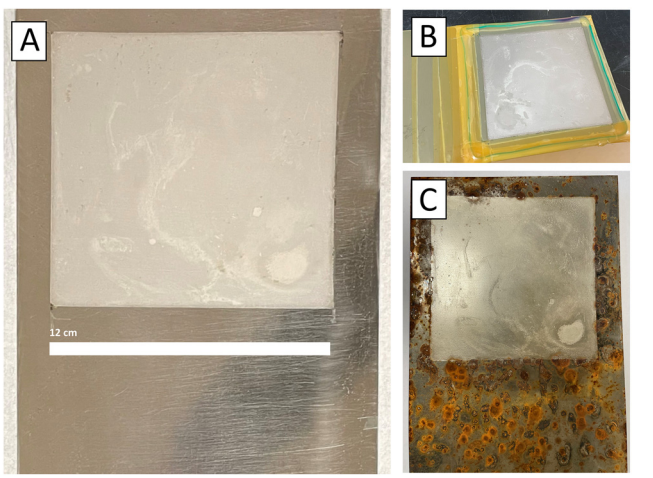

Fig. 9 Photographs of a large area (144 cm^2) electrostamped nickel plating on a steel sheet following sanding, polishing [A] and taping off the edges [B] including a 70 day exposure to ambient outside environmental conditions during July and August 2024 in Patuxent River, Maryland [C].

exposed steel, whereas the nickel-plated area remained unaffected (Fig. 9C). This corrosion test indicates that nickel was deposited successfully and uniformly in the desired area, and that the electrostamping spot plating technique provided corrosion resistance to the workpiece as has been demonstrated by other electrodeposited metals and their alloys.[51–54] Because this deposition did not require submerging the item in a liquid bath, this method could be expanded to larger items including machinery, building materials, automobiles or aircraft without the need for dissasembly.

Typically, applications where a plating repair is needed for large machinery, the part is removed for plating, and this can be addressed with electrochemical marking techniques.[55,56] However, while brush and jet plating maintain an important niche for repairing and restoring parts, these established methods remain limited by their reliance on a continuous flow of aqueous electrolyte.

In order to reduce the waste and the flow of liquid electrolyte from these commonly used electroplating processes, a novel plating method, as presented here, is required to reduce excess liquid waste while promoting a new level of versatility in manufacturing. This method, as demonstrated in this report could be used to (1) spot plate a variety of metals without submerging the item in a bath, (2) while using pure or mixed alloy metal precursor salts, and (3) would result in a minimal amount of liquid waste.

Electrostamping liquid waste comparison

Industrial bath electroplating is regulated by the 1977 US Clean Water Act (CWA) where plants discharge aqueous waste into public municipal treatment systems or directly in to waters of such as streams, lakes or oceans. Large plants with a daily flow greater than 38 000 liters per day are more heavily regulated for metal and total toxic organic discharge; however there also is some economic advantage to recovering unused metals in addition to environmental considerations.[57,58] Typical bath plating operation involves dipping in alkaline and acidic substrate preparation baths prior to submersion of the work piece in the coating baths, followed by a series of ''dragout'' rinses employed to recover residual metal ions adhered to the surface as the part is removed from the bath. As the plating bath ages, the metal ion source is replenished with the addition of concentrated stock solution, which could be reclaimed by performing evaporative concentrating of the rinse solutions either in air or under vacuum. The bulk of the unused metal byproducts can be reclaimed either through filtration, precipitation or evaporation to form concentrated semi-solid waste sludge, mostly consisting of insoluble metal hydroxides that precipitate out of solution. This waste is processed as hazardous material; whereas liquid effluent waste can be disposed into public water treatment systems if the liquid metal concentrations are below the limits set by the CWA. For example, under best practical control of existing sources, nickel metal waste must be limited to 54.85 mg m^{-2} of area coated per day for metal preparation and less than 21.21 mg m^{-2} of area coated per day for coating operation. Standard Watt's nickel plating operates with bath concentrations of 60 g L^{-1}–89 g L^{-1} of Ni^{2+} metal.[3]

By comparison, electrostamping of nickel operates at substantially higher plating concentrations (Ex. 355 g L^{-1} Ni^{2+}) equating to an average of 4.76 times more nickel plating mass per volume of electrolyte.[21] To estimate this, for the 144 cm^2 large area nickel plating demonstration (Fig. 8), the remaining paste was collected, stored, and the coupon was rinsed to collect the dragout. No attempt was made to reconstitute the dragout for recycling. The dried byproduct had a mass 0.20 ± 0.01 mg (13.88 mg m^{-2}) Ni^{2+}, indicating a 34% reduction in waste compared to the best practice control standard limit for bath plating. Because the electrolyte plating paste can be easily removed following each deposition; the process we report here also eliminates the need to manage large volumes of hazardous aqueous material.

Considerations and limitations

In order to draw a contrast between electrostamping and traditional aqueous bath plating and understand possible future research directions, several aspects are considered including the choice of electrolyte ingredients, primary and secondary reactions, limitations, and the electrostamping cell design as it may be adapted for various engineering applications that require patterned marking of metal deposits.

Recipes and additives. The ingredients for the electrolyte pastes were adapted from traditional bath plating, where reagents were concentrated to a viscous aqueous paste. Specifically, nickel plating followed Watt's recipe (1 : 5 : 1 molar ratio of nickel sulfate, nickel chloride and boric acid, respectively).[3] Likewise, a copper sulfate/sulfuric acid solution is popular for copper plating;[35,59] however, we observed higher quality coatings from pastes containing a copper sulfate/water mixture. Zinc paste (1 : 1 molar ratio of zinc chloride and boric acid) was adapted from recipes that also contain KCl/NH_4Cl,[36,59] although these additives were omitted in the electrostamping recipe because co-deposition of these crystalline salts were observed in the zinc deposit matrix due to precipitation from the concentrated electrolyte. For this reason, additives were generally omitted in order to control for pure metal deposition without unintended variables. In contrast, boric acid was found to be an essential additive as a pH buffer for both nickel and zinc plating. Tin was plated following recipes containing tin sulfate where a viscous paste was formed using concentrated sulfuric acid.[37,59] Because additives are an essential part of the electroplating industry to impart quality to the plating (*e.g.* brighteners, levellers, wetting agents, complexing agents), an opportunity exists to explore the adaptation and optimization of additive content in aqueous paste electrolytes.

Primary and secondary reactions. Target reactions of electroplating include reduction of metal ions to solid metal at the cathode (eqn (S1)–(S4)) and metal oxidation at the anode (eqn (S5)) to provide charge balance. The hydrogen evolution reaction (HER) is a competing secondary reaction, especially in acid conditions (E° = 0.00 V SHE, eqn (S6)) *vs.* basic conditions (E° = −0.828 V SHE, eqn (S7)). Oxygen evolution is less likely due to its high minimum potential (E° = −1.23 V, eqn (S8)). Compared to liquid plating, the molarity of metal ions [M^{2+}] in

the electrostamping electrolyte is ~4.76 times more concentrated and therefore the spontaneity of the metal reduction should be improved as described by the Nernst equation where n = metal ion valence (eqn (4)).

$$E_{(298\,\mathrm{K})} = E^{\circ} - \frac{0.059}{n}\log\frac{1}{[\mathrm{M}^{2+}]} \quad (4)$$

Using electrostamping nickel as an example (355 g L^{-1}, 6.05 M Ni^{2+}) *vs.* Watt's average Ni^{2+} concentration (1.28 M), one would expect a potential change of +0.474 V and a favorable Gibbs free energy change of −3.86 kJ mol^{-1}.

At the same time, due to the viscosity of the electrolyte paste, mass transport at the cathode may be limiting, and several major implications should be considered. For example, local pH at the cathode may increase due to the build-up of spectator anions following metal deposition. Sulfate and chloride are very weak bases and would not be expected to contribute significantly to the formation of hydroxide ions (eqn (S9)). However, hydroxide formation from the reduction of water (eqn (S8)) is possible, which could contribute to the precipitation of insoluble metal hydroxides (eqn (S10)). However, this is less likely in acidic conditions of Sn plating. In addition, boric acid used here for nickel and zinc plating is important for pH suppression following the reduction of water, providing a buffered system to remove excess hydroxide ions (eqn (S11)). However, in a stagnant electrolyte, mass transport of the boric acid/borate conjugates may be limited. In addition, the HER may produce trapped $H_{2(g)}$ at the cathode and over time this may result in uneven deposits, although the morphology expected from gas bubbles was not observed in the optical microscopy or AFM images. Similarly, slow mass transport of counter ions from the cathode to the anode may also be restricting the charge balance equilibrium in the cell. On the other hand, electrolyte conductivity is expected to be higher in these concentrated pastes, which may provide some relief to charge imbalances through the wet porous barrier. Additionaly, galvanic displacement during the set-up and prior to applying current, may introduce contaminate cathode ions into the electrolyte paste. In the case reported here, nickel substrates would be expected to initially introduce Ni^{2+} ions into the Cu^{2+} and Sn^{2+} paste but not for Ni^{2+} or Zn^{2+} due to unfavorable standard reduction potentials. Mechanistic studies of the stages of metal deposition from stagnant electrolyte pastes (mass transport, charge transfer, nucleation and growth) would be interesting for future research.

Limitations. Along with the capabilities of plating without a bath, some trade-offs are worth considering when compared to decades of research and development of traditional electroplating. For example, the stagnant electrolyte is a key element of electrostamping, however, a continuously flowing/mixing electrolyte has proven advantages over control of the plating system. Electrostamping may provide challenges and opportunities to optimize stagnant conditions by addressing potential counter-ion accumulation, hydrogen gas evolution, the monitoring and adjustment of pH, electrolyte composition, temperature, and heat transfer. More characterization is also needed including direct thickness measurements *vs.* calcuated thickness from deposit mass to characterize uniformity in thickess, Hull cells to understand uniformity in current density and current/voltage studies to determine the thermodynamic, kinetic and ohmic contributions of cell voltages and probe the fundamentals and mechanisms of deposition.[59]

Cell design. In this proof of concept study, a flat parallel plate design was tested to provide simplicity, operational convenience and uniform current distribution. However, the structure could be adapted to complex cathode geometries using custom anodes. With an electrolyte thickness of 2–5 mm, the anode design could be tailored to follow the contours of the workpiece and/or scaled up to large areas (Ex. Fig. 9). Compatibility with industrial processing includes the reusability of the electrolyte paste, a reduction in liquid waste management, and the ability to plate the surface of an object without submersion.

Others have envisioned electroplating methods that also do not involve the traditional submerging of the workpiece in the electrolyte. As previously mentioned, commonly used brush and jet plating procedures that are convenient for repair of machine parts where the dilute electrolyte is passed over the workpiece under constant flow.[13,60] In another example, Long *et al.* teaches of brush plating on the cathode that is first layered with a nylon membrane to trap composite particles onto compressor blade tips.[60] Van der Pyl devised a rigid custom anode holder to plate from a contained liquid electrolyte[61] and Anderson attached a tray to hold a liquid electrolyte *via* gravity onto a cathode surface to provide surface plating confined to the target area.[62] In contrast to these methods, the electrostamping method reported here contains highly concentrated viscous and stagnant electrolytes without continuous flow that can be pasted onto a surface regardless of orientation, and can incorporate higher composite loadings.[20,21,63]

On an industrial scale, a cost reduction is predicted from removing liquid waste management, and the power requirements were found to be equivalent to bath plating. For example, nickel electrostamping required ~1.6 V at 0.02 A cm^{-2} to plate onto a 9 cm^2 substrate (Fig. 4A) equating to 0.288 W and 0.33 Wh over 20 min, plating approximately 8 μm (Fig. S7A), which matches Watt's nickel plating.[3] Finally, the simplicity of the cell design and low profile may provide advantages for thermal management, print/stamping onto electronic components or adapting to large or irregular surfaces.

Conclusions

A novel electrostamping electroplating technique was demonstrated for its potential as an alternative to bath plating for nickel, copper, zinc and tin. Dehydrated aqueous metal salts containing approximately 4.76 times less liquid electrolyte than traditional bath plating were painted on top of nickel foil substrates and metal ions were reduced *via* constant current chronopotentiometry. All metals deposited were crystalline, phase-verified with X-ray diffraction and were relatively smooth (246 ± 68 (Ni), 356 ± 100 (Cu), 842 ± 228 (Zn), 864 ± 312 (Sn) nm RMS) as measured by atomic force microscopy. Surface morphology was visualized with optical microscopy to reveal uniform

surfaces. The expected mass of the films increases for nickel, copper and zinc following Faraday's Law for coating durations of 10 and 20 min, while showing reasonably high cathode current efficiencies (~90%). Tin deposition from sulfuric acid was less stable and may benefit from further research on necessary additives. Alloy mixtures of $Cu^{2+}|Zn^{2+}$ electrolyte pastes were tested for various brass compositions and tuned by controlling excess Zn^{2+} loading. The relationship between Zn^{2+} loading and the resulting plating composition was tracked by X-ray fluorescence spectroscopy. Further research investigating electrostamping of brass is required to optimize the process, including complexing ligands, to account for the large difference in reduction potentials between the two metals. To demonstrate the potential capability of removing a liquid bath, a large area steel sheet was nickel plated. While removing the need for managing large volumes of hazardous liquid materials, objects that are large, irregular, water sensitive, or otherwise incompatible with submerging in a liquid electrolyte, can be plated with this alternative method. Based on the results presented here, electrostamping may provide positive implications for health and safety as well as technological advancements in manufacturing and repair.

Experimental

Reagents

All reagents were used as received from Sigma Aldrich, following drying of the metal salts under vacuum, including $NiSO_4 \cdot 6H_2O$, $NiCl_2 \cdot 4H_2O$, H_3BO_3, $CuSO_4 \cdot 6H_2O$, $ZnCl_2$, $SnSO_4$. Nickel metal foil was used as the cathode, and metal foils of nickel, copper, zinc and tin were used for the anodes all with purity greater than 99.96%. For the large area nickel plating, a 16-gauge weldable solid steel sheet was used (Hillman SteelWorks).

Coating process

For each coating, solid powders were combined based on the following molar ratios: nickel plating [1 : 5 : 1 $NiSO_4 \cdot 6H_2O$: $NiCl_2 \cdot 4H_2O$: H_3BO_3], copper plating [$CuSO_4$], zinc plating [1 : 1 $ZnCl_2$: H_3BO_3], and tin plating [$SnSO_4$]. Anhydrous powders were mixed and ground in a mortar and pestle. To each, enough distilled water was added to produce a thick paste that could be spread onto the cathode. The amount of water in each mixture was recorded as follows for each paste in grams water per mL of paste, except tin where concentrated sulfuric acid replaced water as the solvent: nickel (2.67), copper (1.25), zinc (4.31) and tin (4.61). Brass electrolyte pastes were made by combining pre-mixed copper and zinc salt precursor powders to match the desired molar ratio before adding water. Following water addition, the concentrated pastes were set to rest for 24 hours before application to allow for heat dissipation and volume expansion resulting from the exothermic hydration reaction. The nickel foil (or steel) cathode was cleaned with concentrated KOH using a cotton swab and scrubbed with Kimwipe cleaning paper, rinsed with water, dipped in 10% by vol. HNO_3 for 5 s, and rinsed with water before placing in a 3D printed PLA holder, or a surface section was taped off using platers tape. The electrolyte paste was then applied to this metal surface and agitated with tapping to remove trapped air from the paste. To do this, a metal scoopula was tapped on the surface of the item around the plating area 5–10 times or until no additional bubbles were observed. Finally, the anode foil (Ni, Cu, Zn or Sn to match the metal to be plated) with area to match the cathode was cleaned with concentrated KOH, rinsed with water, dipped in 50% by vol. HNO_3 for 5 s and then rinsed with water. A potential was applied between the anode and the cathode with a Tekpower TP3005T variable linear DC power supply. Electrical contact with the electrodes was made with either alligator clips or by soldering on a wire. The plating was conducted under constant current mode, and the initial voltage was determined by adjusting the current. After coating with a stagnant electrolyte for 10 or 20 min at 5, 10 or 20 mA cm^{-2}, the samples were removed from the set-up, washed with water, wiped clean, and dried. Personal protective equipment including googles, nitrile gloves, laboratory attire and access to a fume hood is required for handling metal salts and concentrated acid/base solutions.

Characterization

Coated sample surfaces were digitally photographed by optical microscopy using a Nikon Eclipse 80i model where samples were top-illuminated. Images were collected without post-processing, following light saturation and contrast optimization with Zeiss ZEN Blue software to increase focus and image quality. Nanoscale surface morphology was characterized by a Nanosurf Naio atomic force microscope (AFM). Surface area roughness values (Sa) represent the arithmetical mean height deviations of the surface, and were calculated from the 3D topographical data from the 50 × 50 μm *z*-height AFM images with 256 points per line. Images did not undergo any post-processing following acquisition. X-ray diffraction (XRD) patterns were taken with a Bruker D8 Advance X-ray diffractometer with 0.6 mm slit 0.25 s per step 0.241 degrees step size per step, 400 steps (fast scan) and 2000 steps (slow scan) using the configuration of coupled two theta/theta continuous PSD fast from 4–100 degrees 2θ, no oscillation, λ = 1.5406 Å/1.54439 Å Cu Kα_1 and Kα_2, respectively, with 40.0 kV and 25 mA. Electrochemical measurements were taken with a calibrated Gamry 1000E potentiostat. A platinum wire was used as a pseudo reference and placed between the anode and cathode. Constant current mode was monitored *via* chronopotentiometry. Cu|Zn atomic ratios were verified with a 200 W, 48 kV Spectro Midex ED-XRF X-ray fluorescence spectrometer calibrated to brass standards.

Author contributions

AA-P, JH, AD, AH: experimentation, analysis and writing. JS and TT: conceptualization. TT: funding acquisition, analysis, supervision, writing and visualization.

Conflicts of interest

There are no conflicts to declare.

Data availability

The data supporting this article have been included as part of the supplementary information (SI). Supplementary information: Figures S1–S10, and raw spectral data. See DOI: https://doi.org/10.1039/d6ma00854b.

Acknowledgements

This material is based upon work supported by the National Science Foundation under Grant No. 2305503. Any opinions, findings and conclusions or recommendations expressed in this material are those of the authors and do not necessarily reflect the views of the National Science Foundation.

References

1 Y. Kulkarni, *Electroplating Market Analysis: Demand Surge Across Automotive, Electronics and Industrial Sectors, Precedence Research*, **4642**, 2025.
2 W. Giurlani, G. Zangari, F. Gambinossi, M. Passaponti, E. Salvietti, F. Di Benedetto, S. Caporali and M. Innocenti, *Coatings*, 2018, **8**, 260.
3 W. Lo, *Nickel Plating Handbook*, The Nickel Institute, 2023.
4 M. Ganapathi, S. V. Eliseeva, N. R. Brooks, D. Soccol, J. Fransaer and K. Binnemans, *J. Mater. Chem.*, 2012, **22**, 5514–5522.
5 X. Li and K. Binnemans, *Chem. Rev.*, 2021, **121**, 4506–4530.
6 W. Simka, D. Puszczyk and G. Nawrat, *Electrochim. Acta*, 2009, **54**, 5307–5319.
7 S. Rajoria, M. Vashishtha and V. K. Sangal, *Environ. Sci. Pollut. Res.*, 2022, **29**, 72196–72246.
8 M. T. Kamar, H. Elattar, A. S. Mahmoud, R. W. Peters and M. K. Mostafa, *Int. J. Environ. Anal. Chem.*, 2024, **104**, 4143–4176.
9 M. T. A. Reis and M. R. C. Ismael, *Phys. Sci. Rev.*, 2018, **3**, 1–24.
10 A. Agrawal and K. K. Sahu, *J. Hazard. Mater.*, 2009, **171**, 61–75.
11 D. M. Mattox, *Met. Finish.*, 2002, **100**, 394–408.
12 B. A. Schwartz, *US Pat.*, US3313715A, 1961.
13 E. M. Zimmerman, *US Pat.*, US2854387A, 1957.
14 N. Singh, H. Siddiqui, B. S. R. Koyalada, A. Mandal, V. Chauhan, S. Natarajan, S. Kumar, M. Goswami and S. Kumar, *Met. Mater. Int.*, 2023, **29**, 2119–2136.
15 Q. Huang and Y. Zhu, *Adv. Mater. Technol.*, 2019, **4**, 1800546.
16 J. De Luccia, *in 32nd Structures, Structural Dynamics, and Materials Conference*, Baltimore, 1991.
17 K. E. H. Marks and W. Ronald, *Estimating Aircraft Depot Maintenance Costs*, Rand Corp, Santa Monica, 1981.
18 N. Ebrahimi, M. Khanlarian, M. Momeni, L. Ahmadi and D. Gallant, *J. Coat. Technol. Res.*, 2025, **22**, 2293–2312.
19 J. R. Adsetts, N. Ebrahimi, J. Zhang, F. Jalaei and J. J. Noël, *Coatings*, 2023, **13**, 850.
20 C. N. Gerwitz, H. M. David, Y. Yan, J. P. Shaw and T. K. Townsend, *Adv. Mater. Interfaces*, 2020, **7**, 1901282.
21 J. Hancock, C. Russell, J. P. Shaw and T. Townsend, *JoVE*, 2020, e61484, DOI: 10.3791/61484.
22 M. D. Feldstein, *US Pat.*, US20120021120A1, 2012.
23 M. D. Feldstein, *Met. Finish.*, 1999, **97**, 87–90.
24 N. Feldstein, *US Pat.*, US5514479A, 1996.
25 N. Feldstein, *US Pat.*, US5834065A, 1998.
26 N. Feldstein, T. Lancsek, D. Lindsay and L. Salerno, *Met. Finish.*, 1983, **81**, 35–51.
27 F. C. Walsh and C. Ponce de Leon, *Trans. IMF*, 2014, **92**, 83–98.
28 F. C. Walsh, S. Wang and N. Zhou, *Curr. Opi. Electrochem.*, 2020, **20**, 8–19.
29 Y. He, S. C. Wang, F. C. Walsh, W. S. Li, L. He and P. A. S. Reed, *RSC Adv.*, 2015, **5**, 42965–42970.
30 H. E. Swanson and E. Tatge, *Standard X-ray Diffraction Powder Patterns*, United States Department of Commerce, 1953, vol. 1, pp. 1–95.
31 J. W. Arblaster, *Selected Values of the Crystallographic Properties of the Elements*, ASM International, Materials Park, Ohio, 2018.
32 M. Faraday, *Philos. Trans. R. Soc. London*, 1834, 77–122.
33 E. Ilgar, *US Pat.*, US5814202A, 1998.
34 G. A. Di Bari, *Modern Electroplating*, 2010, ch. 3, pp. 79–114.
35 J. W. Dini and D. D. Snyder, *Modern Electroplating*, 2010, ch. 2, pp. 33–78.
36 R. Winand, *Modern Electroplating*, 2010, ch. 10, pp. 285–307.
37 F. C. Walsh and C. T. J. Low, *Surf. Coat. Technol.*, 2016, **288**, 79–94.
38 M. Jordan, *Modern Electroplating*, 2010, ch. 9, pp. 265–284.
39 J. A. V. Butler, *Trans. Faraday Soc.*, 1924, **19**, 729–733.
40 R. A. McCoy, *Standard Experiments in Engineering Materials Science and Technology*, NASA Langley Research Center, National Educators' Workshop, 1992.
41 A. Brenner, *Electrodeposition of Alloys: Principles and Practice*, Academic Press, London, 1963.
42 H. P. Coats, *Trans. Electrochem. Soc.*, 1941, **80**, 445.
43 K. S. Barros, E. M. Ortega, V. Pérez-Herranz and D. C. R. Espinosa, *J. Electroanal. Chem.*, 2020, **865**, 114129.
44 M. A. M. Ibrahim and R. S. Bakdash, *Int. J. Electrochem. Sci.*, 2015, **10**, 9666–9677.
45 H. E. Swanson and R. K. Fuyat, *Standard X-Ray Diffraction Powder Patterns*, United States Department of Commerce, 1953, vol. 2, pp. 1–63.
46 A. Modrić-Šahbazović, A. Smajlagić, Z. Sakić, M. Novaković, N. Latas, M. Popović, M. Đekić, S. Isaković and A. Salčinović Fetić, *J. Cryst. Grow.*, 2025, **650**, 128003.
47 J. L. Ong, D. W. Farley and B. K. Norling, *Dent. Mater.*, 2000, **16**, 20–25.
48 W. H. S. Bragg and W. L. S. Bragg, *Nature*, 1913, **91**, 477.
49 O. Antonoglou, E. Founta, V. Karagkounis, E. Pavlidou, G. Litsardakis, S. Mourdikoudis, N. T. K. Thanh and C. Dendrinou-Samara, *Front. Chem.*, 2019, **7**, 817.
50 L. Vegard, *Z. Phys.*, 1921, **5**, 17–26.
51 S. Priyadarshini, R. S. Bhat, A. G. Bindu, P. Nagaraj and P. D. Rekha, *Results Surf. Interfaces*, 2025, **18**, 100402.
52 S. Priyadarshini, R. S. Bhat, A. G. Bindu, P. Nagaraj and P. D. Rekha, *J. Mater. Eng. Perform.*, 2025, **35**, 8511–8524.

53 R. S. Bhat, P. Nagaraj and S. Priyadarshini, *Surf. Eng.*, 2021, **37**, 755–763.
54 R. Bhat and A. Chitharanjan Hegde, *J. Met., Mater. Miner.*, 2025, **35**, e2218.
55 A. A. Ghobbar, *Aircraft Maintenance Engineering*, Wiley, 2010, DOI: 10.1002/9780470686652.eae552.
56 S. K. Weerasekera, *Introduction to Maintenance, Repair and Overhaul of Aircraft, Engines and Components*, SAE International, 2020.
57 D. M. Costle, S. Davis, R. B. Schaffer, E. P. Hall and J. B. Hanson, *Development Document for Existing Source Pretreatment Standards for the Electroplating Point Source Category*, US Environmental Protection Agency, Washington, DC, 1979.
58 US Code 40 CFR Part 413.
59 D. Pletcher and F. C. Walsh, *Industrial Electrochemistry*, 2nd edn, Springer, Dordrecht, 1993.
60 K. C. Long, B. A. Manty and C. C. McComas, *US Pat.*, US5389228A, 1995.
61 E. Van Der Pyl, *US Pat.*, US2391206A, 1942.
62 E. K. Anderson, *CN Pat.*, CN107142514B, 2021.
63 J. Shaw, Y. Yan and T. Townsend, *US Pat.*, US11519091B2, 2022.